

Thomas Müller¹ & Volker Gollnick¹

¹Institute of Air Transportation Systems, Hamburg University of Technology

Abstract

Generally, prototyping goes hand in hand with additive manufacturing technologies. Especially in the construction of unmanned aerial vehicles (UAV), these rapid prototyping methods are a key to quickly obtaining a functional prototype. The Institute of Air Transportation Systems is working on an innovative vertical take-off and landing (VTOL) model in the 25 kg weight class. The main airframe is intended to be built from composite materials in combination with each other and/or with the help of 3D printing materials. This article details the construction methods for the structure of the proposed aircraft. A main focus lies on the implementation of 3D printing methods, mainly via Fused Deposition Modelling (FDM) and different types of plastic as printing material, to derive different construction methods, including composite hybrid structures, for the respective structural components. In addition, issues on structural design, load tests and final results of the efforts are presented. This paper is intended to be a guide for other developers/researchers, who start prototyping their own serious aircraft builds, without being dependent on conventional machinery.

Keywords: VTOL, Composite Aircraft, Additive Manufacturing, 3D Printing

1. Introduction

The integration of 3D printing technology into unmanned aerial vehicle (UAV) design revolutionised the prototype manufacturing process. By leveraging 3D printing, UAV design becomes more flexible and cost-effective, enabling complex designs that would otherwise be cost-intensive with traditional methods such as milling and turning. This synergy allows rapid prototyping, customisation for different mission requirements, and the creation of lightweight yet robust components, ultimately improving performance while reducing production time and cost. However, aircraft structures require very light yet stiff constructions. 3D printed materials alone, mainly plastics, are not normally able to deliver this performance. Fortunately, as is common in aircraft design, hybrid structures solve this problem. Stiff materials provide the required strength along the load paths, while the 3D printed material can be used in less stressed areas to keep weight and cost down.

As 3D printing is a broad term, this article focuses only on the FDM printing process, which preferentially uses plastic filament to create the final part. The part itself is built up in layers, starting from the bottom of a build plate that increases in thickness with each layer. The plastic is melted from a nozzle and, together with the pre-defined machine tool path, forms the geometry of the part. This printing process is shown in Figure 1, where it prints a wing section made of PETG material.

The aircraft to be built is a model size aircraft, VTOL capable, with a wingspan of approximately 3 m and a maximum take-off mass (MTOM) of 25 kg. The current development status of this aircraft is shown in Figure 2 and is still in an ongoing iterative process at the time of writing. Part of the procedure is to build some components like wings, fuselage, cargo bay and others in a smaller scale to get more accurate values for weight estimates. This includes interfaces for quick disassembly to facilitate transport to and from the test site.

Aircraft structures are commonly made of composite materials such as glass fibre reinforced plastic (GFRP), carbon fibre reinforced plastic (CFRP) or hybrid sandwich structures, which are a combination of both [1]. In hybrid structures, foam cores and/or other textiles can also be used. To produce



Figure 1 – 3D printing process of a wing structure via FDM

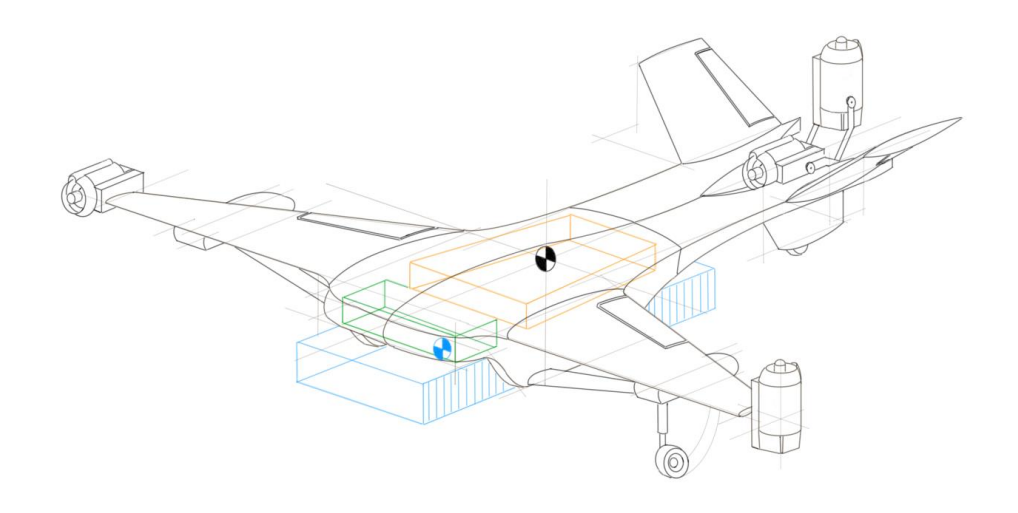


Figure 2 – Concept of the intended VTOL aircraft to be built

such composite structures, moulds are usually required which require CNC machines such as milling and turning machines. A milling machine is typically used to machine the mould for aircraft structures, such as wings or the fuselage. Ideally, the moulds are made from a single piece that is essentially a negative of the structural component. Unfortunately, this requires the machine bed to be at least as long as the length of the part, e.g. half the span of a proposed wing. Alternatively, the moulds can be split into smaller sections, but this requires more machining time for the alignment holes.

Consequently, when relying on external machines, the design must be very accurate and well planned within the project schedule to obtain the required tooling. This also leads to less scope for iterative design improvements due to the more difficult hurdles involved. This challenge provides the basis for implementing 3D printing technology into the structural part design and mould making process.

This paper aims to explore how 3D printing can be used to create a suitable aircraft structure, highlight the advantages and disadvantages of each developed construction method, and provide a guide for other aircraft designers wishing to incorporate additive manufacturing into their designs.

2. Related Works

Below is a summary of other research where 3D printing is being used for similar applications to the work presented.

In [2], a model-size RC aircraft is developed using FDM 3D printing and compared to conventionally made (composite, wood) aircraft. They recommend PET and ABS as suitable printing materials. The printed structures required a minimum wall thickness of 0.6mm. They also point out that the maximum aspect ratio of 12 for the wing should not be exceeded, as beyond this, the torsional stiffness would

start to deteriorate.

[3] gives an overview of 3D printing applications for aerospace parts. Model-size aircraft have been made from PLA and ABS that contain carbon fibre particles. These would lead to better crack and impact resistance. In addition, the process replaces CNC (Computerised Numerical Control) manufacturing, resulting in shorter lead times and lower costs.

In [4], a PVB filament from Polymaker is used to print moulds for carbon fibre lamination. A notable feature of PVB is that it reacts with isopropanol, which can be used to smooth the surface of the printed material. The alcohol evaporates, creating a fine mist that smooths the surface. A mould accuracy of 0.05mm has been achieved. A drawback is the high cost of the material and the sensitivity of the evaporation time. However, it eliminates the need for finishing, such as grinding, on the mould. A similar research approach can also be found in [5].

In [6] different printed moulds are analysed and compared with conventional moulds. One mould was made from PLA and the other from ABS. Both were coated with a mixture of epoxy and gelcoat. The epoxy coating of the PLA mould also contained aluminium powder to improve stiffness. The moulds were then sanded and polished. Interestingly, the cost of the moulds was about 1/10th of the cost of the conventionally milled moulds, with similar lead times. The surface finish of the finished CFRP product found to be best with the PLA mould.

Similarly, [7] also analysed 3D-printed moulds coated with epoxy to make the mould stiffer but also more temperature-resistant for use in an autoclave.

[8] explains 3D printed mould making for moulds that are larger than the dimensions of the printer. It focuses on joints and intersections, how they are connected and what kind of post-processing is required. The resulting composite part measures 1.2m by 0.34m and is intended for a motorcycle cover.

In [9], sandwich structures were created using 3D printed core materials together with CFRP skin layers. These parts are designed to replace conventional aircraft parts and improve impact resistance in the event of a bird strike. The core material was printed in a honeycomb structure to save additional weight.

A comprehensive literature on composite structures with a focus on 3D printing and its integration can be found in [10]. It also covers sandwich structures with 3D printed core materials.

3. Construction Approach

The following subsections contain the theoretical background for the construction of corresponding structural parts. Firstly, a suitable structural part is defined along with the requirements. This is followed by the definition of three construction methods, which form the basis for further analysis. A preliminary evaluation of these methods concludes this subsection with an outlook on which method is suitable for certain types of components. Finally, the materials considered are presented along with their appropriate applications.

3.1 Wing Geometry

The structure of an aircraft can be divided into several main structural groups such as wing, empennage, fuselage, nacelle and landing gear. As the wing is one of the major parts with approximately 1/3rd of the total structural mass of an UAV, a wing structure is selected for further analysis.

3.1.1 Requirements

To simplify time and material demands, a smaller wing geometry compared to the wing geometry of the actual aircraft is considered for analysis. In addition, functional mechanisms such as flaps, ailerons and cable ducts are added to highlight potential issues for the construction method. Actuators and their mechanism are replaced by fixed flange parts as the research focuses on the structure itself.

Regarding the airfoil, a NACA 6716 and a NACA 4416 are considered as shown in Figure 3. Both profiles are known for their forgiving stall characteristics and very high lift coefficients. Aerodynamic data for both airfoils can be taken from [12]. For this work, the NACA 4416 was selected from the

larger flat area on the lower wing. This is useful in several situations, as a flat surface, such as a table, can always be used as a reference or to align the spanwise segments.

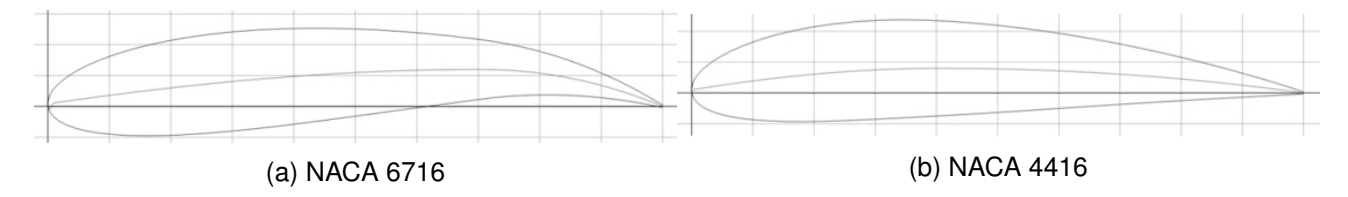


Figure 3 – Considered NACA airfoils [11]

A main spar with constant round geometry is used.¹ This spar is designed to transmit the lift forces during hover (with the engines mounted on the wingtips) and cruise flight. An auxiliary spar with a constant round geometry is also used to secure the alignment and transfer torsional forces. However, the auxiliary spar will only reach half the span.

Table 1 lists all requirements and geometry data for the selected wing organized in related sections. Figure 4 shows a CAD design of the desired wing geometry.

Requirement	Description / Value	Unit
Geometry		
span	800	mm
depth root	300	mm
•	200	
depth tip		mm
airfoil	NACA 4416	
Strength		
main spar	round CFRP Ø25	
aux. spar	round CFRP Ø20	
aux. spai	Touria Of Till \$20	
Feasibility		
spanwise kink	not continuous, step in geometry	
flaps	installability check	
aileron	installability check	
cable channel	must include	
segmented	simulate too small printer	
segmented	Simulate too Sinali printel	

Table 1 – Requirements for the wing structure

3.1.2 Load Cases

For later testing, it is necessary to define the loads to be carried by the structure. As the intended aircraft is a VTOL, hover flight must be considered. Cruise flight and a slower flight with extended flaps are considered. All flights are considered at sea level with an air density ρ of 1.225 kg/m^3 . Cruise flight is performed at 120 km/h with a bank angle of 60°. This will increase the wing loading with Equation 1 from [13] by a factor of 2 for the load factor $n_{Z,bank}$. Generally, load factors for reconnaissance UAVs should be selected according to [13] as $n_{lim,pos}$ =+3 and $n_{lim,neg}$ =-1.

$$n_{Z,bank} = \frac{1}{cos(\phi_{bank})} \tag{1}$$

¹Comparison of square vs. round geometry shows a mass reduction of a factor of 2.1 for a CFRP spar (with equal outer dimension), but costs are approximately four times higher

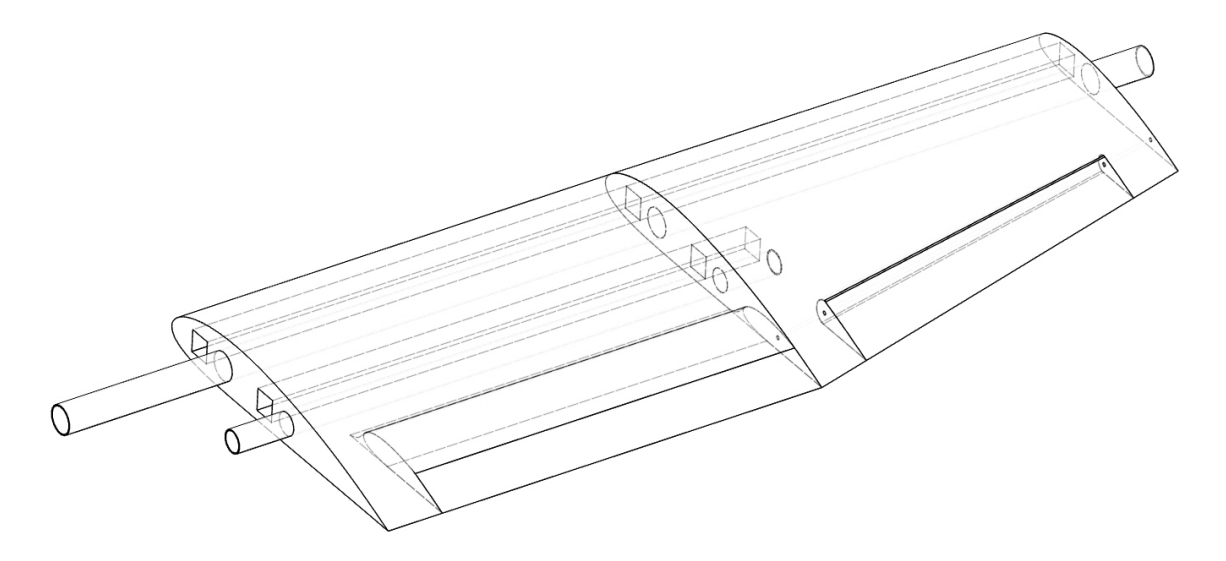


Figure 4 – Intended wing structure to be built

The angle of incidence of the airfoil is 4°, resulting in a lift coefficient c_l of 0.8. The maximum lift coefficient $c_{l,max}$ is 1.6 at an Angle of Attack (AOA) of 14°. The lift coefficient of the airfoil is transformed to the lift coefficient c_L for the whole wing using the Equation 2 from [14]. The same applies to the other coefficients (max, flaps extended) as well as the moment coefficient c_m . Note that Λ is the aspect ratio of the wing and was selected to be 10.

$$c_L = c_l \cdot \frac{\Lambda}{\Lambda + 3} \tag{2}$$

The lift L and the pitching moment M can be calculated using the Equation 3 & 4 from [13]. l_{MAC} in Equation 4 is the mean aerodynamic chord of the equivalent rectangular wing. Drag forces are neglected, as they typically add only tenths of the lift forces. Lift forces clearly dominate.

$$L = \frac{\rho}{2} \cdot v^2 \cdot c_L \cdot S_{Wing} \tag{3}$$

$$M = \frac{\rho}{2} \cdot v^2 \cdot c_M \cdot S_{Wing} \cdot l_{MAC} \tag{4}$$

Table 2 lists all the forces that occur and their respective inputs. The lift distribution can be approximated using the Equation 5 according to Schrenk [15] [16]. This is used to gather the equivalent forces and moments distribution during the loading tests. ²

$$c_l(y) = \frac{1}{2} \cdot c_L \cdot \left[(l(y) + \frac{4 \cdot S_{Wing}}{\pi \cdot h} \sqrt[2]{1 - (\frac{2y}{h})^2} \right]$$
 (5)

3.1.3 Research Interest

The research interest lies on the feasibility of each method and the problems likely to be encountered. The weight of each component is also of interest, as is the cost of the parts themselves and cost of any required moulds.

Finally, the resulting torsional stiffness of each wing is analysed. As each method uses the same size of main and auxiliary spar, the spanwise bending behaviour will not vary much.³ To ensure a comparable basis, the number of skin layers is kept same for all methods. Also, a thinner GFRP skin is selected to increase measurement deflections during load testing.

²y is the spanwise run variable; b is the span of the complete wing, in this case 1.6m; I(y) is the local wing depth.

³For the selected Ø25 mm main spar, considered a load during hover of 100N, the safety factor would still be at 4.6

		Flight State			
Parameter	Unit	Hover	Cruise	Flaps	
Lift	Ν	100	92	108	
Moment	Nm	0	-2.54	-4.10	
Attack Point		tip	distributed	distributed	
ρ	kg/m^3	1.225	1.225	1.225	
V	km/h	0	120	80	
c_l	-	0	0.8	1.2/3.6	
c_m	-	0	-0.08	-0.08/-0.64	
AOA	0	4	4	8	
S_{Wing}	m^2	0.22	0.22	0.22	
Λ	-	10	10	10	
l_{MAC}	m	0.276	0.276	0.276	
n_{load}	-	1.5	3	3	

Table 2 – Loads on the wing during different flight states

3.2 Preliminary Analysis of Building Methods

The construction methods developed use 3D printing materials and technology, either as structural components or as a base for moulds. Each method is described with estimated material costs and masses, excluding the cost of the initial mould in the first step.

As written in advance, each method uses a Ø25mm tube as main spar and a Ø20mm tube as auxilary spar. Both spars are made of CFRP. The skin layers for the analysis were considered as two layers of 100g/m² GFRP. Other variations are stated at the relevant subchapter of each method. For the preliminary analysis only a straight wing is considered without flaps and ailerons.

3.2.1 M1: Hybrid Foam Core

In the first method, referred to as M1, the wing section consists of a hybrid foam core with a skin of CFRP. The hybrid nature of the foam means that most of the internals are made of foam, but for interfaces, such as the wing to fuselage joint, more rigid printed ribs are considered. The foam structure is usually cut out with a hot wire, either by hand or with the aid of a robotic structure, and also includes cut-outs for the two struts as well as for the cable channels. The outer skin is then applied directly to the foam with the integrated struts. A vacuum bag is used to apply the carbon fibres and resin, sucking out the bubbles and moulding the shape to the foam mould. This is known as positive moulding. According to [17], this method is particularly popular for wing structures. It should be noted that method M1 requires only a few 3D printing, resulting in a very short lead time from the start of production to the final finished part. The stencils of the wing for the foam cutting

process are considered as 3D printed as well as the interfaces with tougher material such as ABS.

For the wing section, this would give a total weight of 738 g/m and a cost of 187 €/m.

3.2.2 M2: Shell with printed Ribs

The second method, referred to as M2 is known as shell construction. It requires at least two moulds for the wing section to produce the required outer skin. The moulds themselves can be 3D printed, with for example ABS, in sections, which can then be combined to form a continuous mould. The skin is subsequently laminated into the mould. This process is called negative moulding. After curing in a vacuum bag, the two skin halves can be prepared for further processing. Prior to this, the internal structures, spars and ribs must be prepared. The ribs can be printed from materials such as ABS. Plug-in joints can be used to create a frame structure. These structures are bonded to the skin halves using a special moulding adhesive.

For the wing structure considered, the M2 method would result in a weight of 851 g/m and a cost of 178 €/m. For the inner ribs, 25 % of the initial weight were added.

3.2.3 M3: 3D-Printed Core

The final method, referred to as M3, consists of the two main struts together with only 3D printed structures. These structures will be made of LW-PLA and will directly include additional internal ribs in the appropriate orientation for printing purposes. The printed structure covers the entire wing area with an approximate height of 150-200mm per part. All these sections must be bonded together. The struts are used as an adjustment aid. Alternatively, adjustment taps can be integrated directly into the printed parts. This method is by far the most suitable in terms of the infrastructure required. The resulting weight of the considered wing section would result in a mass of 1013 g/m and a cost

of 188 €/m. For the additional internal structures of the printed parts, 67 % of the initial weight was added with an assumed design.

3.3 Evaluation of Construction Methods

The advantages and disadvantages of each construction methods are already discussed in previous sections. Table 3 shows the weight methods compared and normalised to each other. It can be seen that method M1 gives the best results in terms of mass for the considered wing.

Feature	Unit	M1	M2	М3
Total mass per meter Ratio compared to group lowest	•		851 115	1013 137
Total costs per meter	€/m	187	178	188

Table 3 – Key figures comparison of the considered building methods

Beyond these quantitative results, if we compare each method to the parts it is best suited to, we can say that M1 is best for wing and tail parts. M2 is suitable for the fuselage, engine cowling and other parts that need space for internal equipment such as tanks, electronics and so on. M3 could be used for payload compartments and hatches as it is the most flexible.

3.4 Considered Printing Materials

3.4.1 Printing Materials

Printing Materials for Structures

LW-PLA, or Lightweight Polyactide, is a popular choice for model aircraft due to its unique properties. Its lower density compared to regular PLA makes it exceptionally light. This is achieved through the material's printing characteristics. As the printing temperature increases, typically above 220 ℃, the material begins to foam, increasing its volume and reducing its density. To compensate for this increase in volume, the flow through the nozzle of the printer is reduced. This process can achieve a mass reduction of approximately 60-65 % [18].

Figure 5 shows an example of a temperature tower typically used to calibrate new materials. It can be seen that as the temperature increases from the bottom up, the material starts to foam, which also changes its appearance.

The material also has its drawbacks, such as the foaming process, which causes the nozzle to ooze during movement where printing should stop. This has led to a printing technique known as vase mode. It allows each layer to be printed with a continuous line without stops, resulting in a clean part that requires no finishing. The latest generation of 3D printers, e.g. Bambulab or FLSun S1, with print speeds of up to 500 mm/s and accelerations of 20,000 m/s², compensate for the bleeding phenomena of LW-PLA to a minimum.



Figure 5 – Temperature tower with colorfabb's LW-PLA [19]

Another disadvantage with the material, as with regular PLA, is its glass transition temperature of around 55 °C. At this temperature, the material begins to soften and lose its strength. For remote controlled (RC) aircraft models, this is usually critical during prolonged exposure to the sun in summer, especially if dark colours are applied to the model.

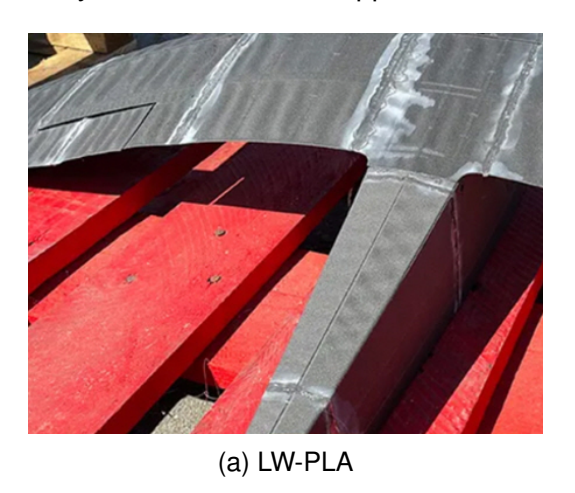




Figure 6 – Comparison of LW-PLA to LW-PLA-HT after 60min exposure time after [20]

The latest developments from the Dutch company colorfabb have created **LW-PLA-HT**, where HT stands for high temperature. According to [20], the glass transition temperature is at least 100 °C. They have also verified it with several tests, as shown for example in Figure 6. The only disadvantage of the material is its higher tendency to warp, which means that the material is sensitive to sudden temperature gradients. Therefore, an enclosed printer is required to print the material.

Another alternative for LW-PLA comes from Polymaker, who offer a pre-foamed material called **Polylite LW-PLA**. This means that there is no active foaming during printing, which eliminates the issue of nozzle leakage during movement. However, the density achieved is only about 30% lower than that of regular PLA [21].

Printing Materials for Moulds

Composites are manufactured through a careful process that begins with the creation of specialised moulds that reflect the negative shape of the actual model. These moulds, typically made from materials such as aluminium, steel or rigid foam sheets, are precisely shaped to reflect the desired structure of the final product. For prototypes, hand-laminated fibres are usually used. Each layer is carefully placed in the mould. Resin is added to each layer to ensure proper adhesion and alignment. Hand tools, rollers and later vacuum bags are used to ensure a strong, bubble-free bond between the layers. After curing, the resulting part can be removed from the mould. During curing, temperatures

can reach up to 55°C, depending on the resin used 4.

Consequently, the mould material should have good machinability, higher temperature resistance and higher strength. These requirements can be met by acrylnitrile-butadiene-styrene copolymer (ABS), a thermoplastic commonly used in various applications. In terms of printing, ABS requires an enclosed printer due to its sensivity to thermal gradients. In addition to its good machinability, it reacts when exposed to acetone, a cleaning agent. Normally, the acetone is evaporated by placing the part in a box together with acetone soaked papers. The outer surface is smoothed and the layer lines removed using this property of ABS. This behaviour can be used to minimise the amount of sanding required to achieve the typical skin of composite parts.

A material with a similar reaction to certain chemicals is **Polysmooth**, from Polymaker. It prints more easily than ABS and is post-processed by exposing the part to an isopropanol mist. Depending on the exposure time, typically between 15-60 min, the smoothness of the part can be adjusted [22].

3.4.2 Comparison Material Properties to Composites

Table 4 lists the material properties of printed materials compared to fiber composites. Obviously, the modulus of elasticity (E-module) of fibers is much higher than that of printed materials. This also means that even if tougher printing materials were used, they would still be the weak point compared to fibers. The focus should therefore be on finding hybrid structures that combine printed material and fiber composites.

Material	Density [kg/m ³]	E-module [N/mm ²]
CFRP	1700 - 1900	230,000 - 700,000
GFRP	2600	60,000 - 130,000
ABS	1050	2200 - 3000
LW-PLA	403 -476	920 - 3250
Polylite LW-PLA	735	2636 ± 330

Table 4 – Comparison of material properties [18] [23] [24] [25]

4. Construction Procedure

In this section, the construction process of each method is shown, along with the problems encountered during construction and the key figures for the individual weights. The final subsection compares all 3 methods.

4.1 M1: Hybrid Foam Core

4.1.1 Stencils Styrofoam

The core material for this method is mainly styrofoam. To get the appropriate shape, a custom built foam cutter is used. The foam cutter consists mainly of aluminium profiles, a piano wire of Ø0.6mm, connectors, a spring, wires, a switch and a laboratory power supply. The device is shown in Figure 7. The wire is guided by a bearing with a V-slot on each side. This reduces wobbling and jumping of the wire during cutting. Additionally, the electrical contact point is positioned inside the elbow to ensure only the inner area is heated. As the wire heats up, the spring will compensate for any increase in wire length. In this setup, a 12V and max 3A power supply was sufficient.

The wire of the foam cutter is guided by stencils of the actual wing shape. To create the entire wing, the order of cuts should be planned before starting. Otherwise there is a risk of cutting away joints earlier than necessary. Figure 8 shows the stencils for the straight part of the wing. The stencils for the top and bottom profiles of the wing have been made in a split design to ensure that there is always a slight force of gravity on the foam cutter against the guide. That makes the cut smoother and easier to achieve. The stencil for the upper mould also contains the guides for the cut-outs for

⁴This only applies to manual lamination of GFRP or CFRP; if prepreg fibres are used, a curing oven is required which uses much higher temperatures





(a) Foam cutter assembly

(b) Zoom in of elbow

Figure 7 – Foam cutter for styrofoam

the spars and cable ducts. All the guide areas of the ABS stencils have been covered with aluminium tape which provides a smoother glide during cutting and acting as a heat barrier to protect the stencil. The stencils themselves were inserted into the edges of the square foam block with an end stop at the front. The design ensures that the guide is already outside the foam before cutting to simplify the cutting process. Transitions are always tangential, allowing for smoother movement.

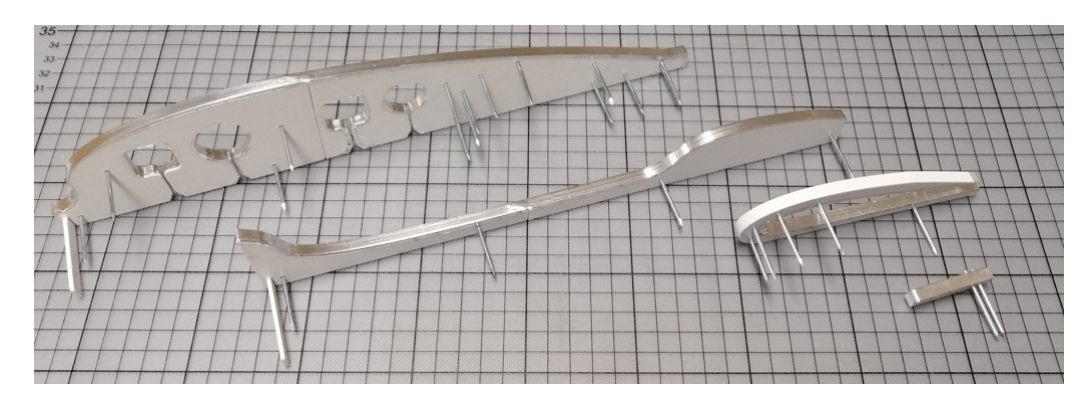


Figure 8 – Stencils for the styrofoam cut of the straight wing part

Regarding the cutouts for the spars and cable ducts, a simple method to analyse the quality of the cut is to analyse the cutout materials, as shown in Figure 9. If a defect occurs, as shown in Figure 9b, another cut will solve the problem. If there is a defect in the outer wing shape, it can also be repaired by sanding or by simply cutting a new core, as the material is relatively inexpensive.



(a) Foam removal after cut



(b) Defect in foam cut out

Figure 9 – Analysis of the foam cut outs

4.1.2 Lamination

Prior to lamination, all wing sections and spars were glued together with a high performance glue filled with cotton flocks. A glue with a higher proportion of cotton flocks was used to fill the gaps in the spar and cable ducts from the cutting process. That increased the amount of glue required. In addition, a thinner slurry of glue with cotton flocks was applied to the styrofoam skin, following the recommendation in [26], as it helps to achieve a better bond with the GFRP skin layers. Figure 10

shows the closed areas of the glued foam core. It is also noticeable that the edges of the wing (root, tip) have printed ABS end plates glued in place to provide an interface for later joints.



Figure 10 – Glued foam sections with the filling of cotton flokes

A band of aramid fiber was applied to the aileron on the upper side of the wing. This acts as a hinge and is typically used in positive form concepts. The cut-outs for the aileron are made after the wing has cured.

Mylar film was used for lamination. The fibreglass is applied directly to the mylar along with the resin on a flat surface. Once all the layers have been applied (here: 1 layer of $50g/m^2$, 1 layer of $163g/m^2$ GFRP), the complete composite is wrapped around the wing. At this stage, the mylar will be quite loose on the wing, requiring continuous pulling on the mylar. According to [27] only a vacuum of -20 kPa should be applied using a normal vacuum cleaner.



(a) Lifted leading edge in pretest



(c) Small lift and air in leading edge



(b) wavy skin



(d) Curved and bend transition in flap area

Figure 11 – Defects with M1 Method

In a pre-test, a vacuum cleaner was used to draw the vacuum. It should be noted that the larger the vacuum bag, the higher the risk of small leaks. The result is that the vacuum cannot be held and, due

to the stiffness of the Mylar, the film begins to lift off the core along with the skin layers. The outcome will be a severe shape defect as shown in Figure 11a. For all subsequent laminations, a continuous vacuum pump with a pressure regulator was used.

Deviations were also found in the final wing. In Figure 11b, it can be seen that the skin follows the natural structure of the foam balls, even with the low vacuum. This could be remedied by using a different foam with finer pores and a higher density. Additionally, Figure 11c shows a slight deviation in the nose area of the wing. Figure 11d illustrates that the foam itself is too weak to form a proper transition at sharp corners resulting in additional printed endplates at such transition areas.

4.1.3 Weight Rating M1

Table 5 presents masses of individual parts to be analysed. Obviously, the skin masses are dominant, but these are roughly the same for each method. In addition, the glue with cotton flocks is one of the larger weight drivers, as all the slots from the foam cutting of the spar and cable ducts need to be filled. In a subsequent test, the slots could be pre-filled with pieces of foam to further reduce the amount of adhesive required.

Part Name	Mass [g]	Ratio to Total [%]
main spar Ø25	108	17.7
2nd spar Ø20	44.4	7.3
styrofoam straight	40.0	6.6
styrofoam angled	34.7	5.7
styrofoam flap	6.3	1.0
ABS enddisc root	25.9	4.3
ABS enddisc top	11.3	1.9
Flap connector (2x)	6.0	1.0
glue with cotton flocks GFRP skin incl. resin	108	17.7
wing	191.7	31.5
flap	32.7	5.4
total mass	609	100

Table 5 – Individual part masses of M1 wing

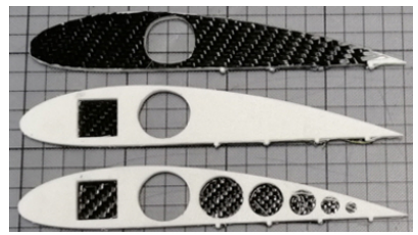
4.2 M2: Shell with printed Ribs

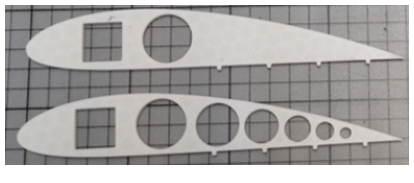
4.2.1 Pretests Ribs

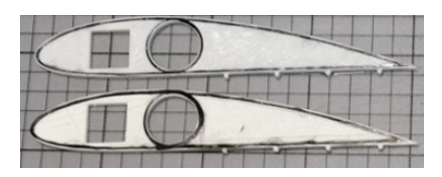
The main stiffness of the M2 is derived from the ribs. Therefore, a pre-test was conducted to determine an optimal material combination and to assess its stiffness. The tested ribs, shown in Figure 12, are as follows: LW-PLA double faced with 1 layer of CFRP, LW-PLA with single sided 1 layer of CFRP, LW-PLA holed with one layer of CFRP, ABS full, ABS holed, LW-PLA full, LW-PLA holed, ABS with CFRP rowings, LW-PLA with CFRP rowings. The size of the ribs matched the rib from the tip of the wing.

ABS ribs were also skinned with CFRP, but adhesion was poor. The CFRP layer could be easily peeled off during a banana test (see Figure 13). Conversely with LW-PLA, the skins could not be separated which indicates that ABS also has a natural separation with composites.

For the test setup, the ribs were evenly distributed on 2 CFRP spars. The spars were force and form fitted into 2 fixtures, as shown in Figure 14. The load was initiated 100mm from the spar position with a bucket suspended from a wire. The bucket was progressively filled with sand. At each filling, the distance from the trailing edge and the angle of the rib at the trailing edge were measured. For this purpose, fixed measuring positions were designed into the test rigs. Twisting of the CFRP spar was also monitored but could be neglected.







(a) CFRP skinned

(b) printed only, full and holed

(c) with CFRP rowings

Figure 12 – Considered ribstyles to be tested



Figure 13 – Banana test with ribskin



Figure 14 – test setup for ribs loadtests

The results of the angle and length measurements were similar. The highest load tested was 2000g, which simulates a torque 8 times higher than that expected during cruise flight for the whole wing. Figure 15 depicts the angle deflection. The rib with the double sided CFRP skinning exhibits the highest stiffness and the ones with CFRP rowing reinforcements also perform well. Ribs with the additional holes collapsed at an earlier stage of the test.

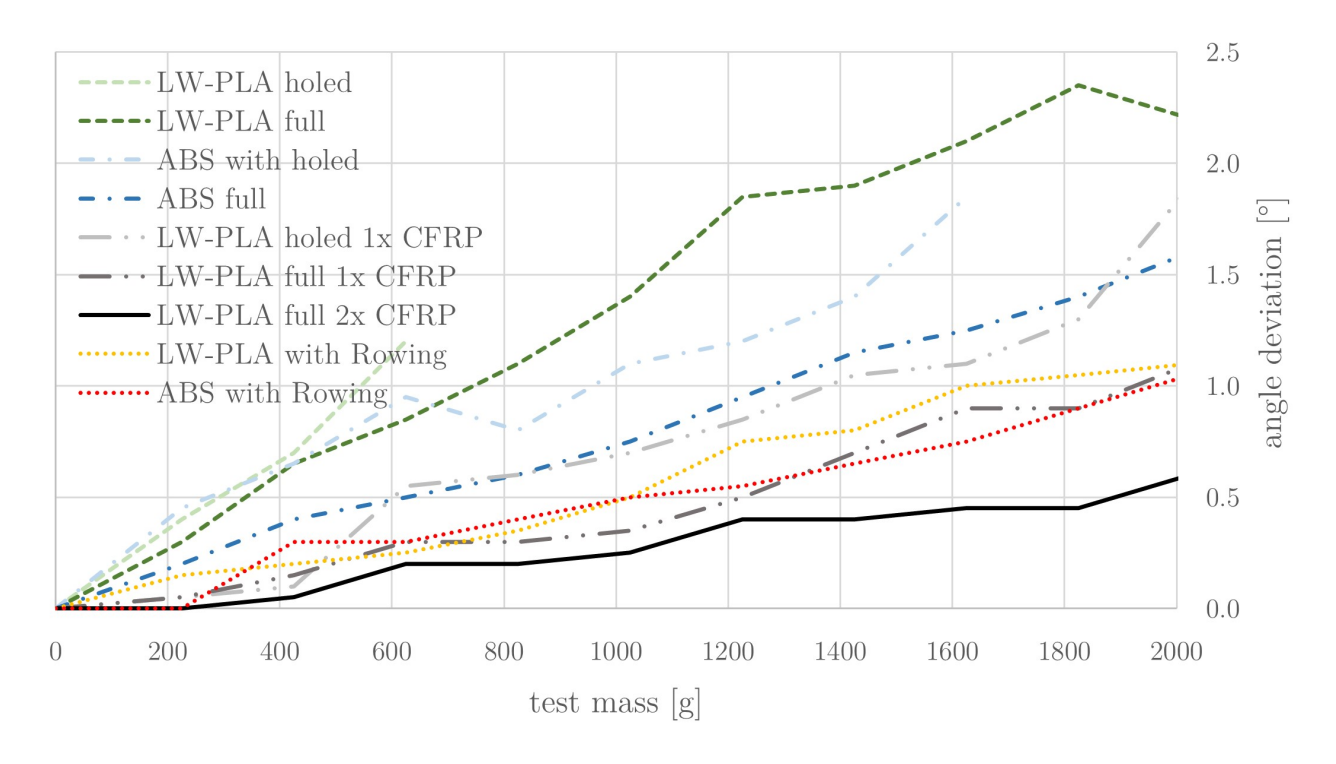


Figure 15 – Angle deviation from rib loadtest

Table 6 lists each rib type together with its weight and stiffness. The LW-PLA with CFRP rowing was chosen as a good compromise between weight and performance.

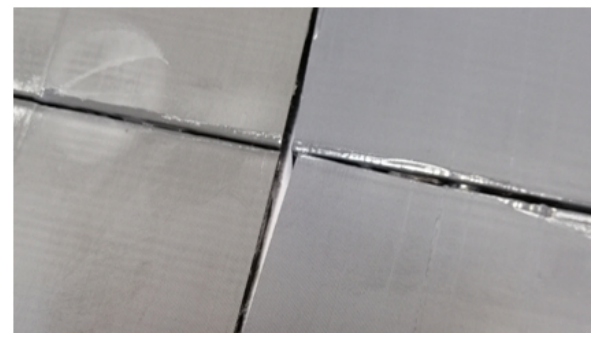
Rib Type	Mass [g]	Ratio to Heaviest [%]	Angle Deflection [°]	Stiffness [%g]
LW-PLA, closed, 2xCFRP	6.49	100	0.6	0.09
LW-PLA, closed, 1xCFRP	5.45	84	1.1	0.2
LW-PLA, holes, 1xCFRP	4.66	72	1.9	0.41
ABS, closed	4.84	75	1.6	0.33
ABS, holes	4.42	68		
LW-PLA, closed	3.71	57	2.2	0.59
LW-PLA, holes	2.91	45		
ABS, Rowing CFRP	6.08	94	1.1	0.17
LW-PLA, Rowing CFRP	4.60	71	1.1	0.24

Table 6 – Individual masses of M2 ribs pretest

4.2.2 Negative Mould

The negative moulds were printed in ABS in multiple sections due to the printer's print space. Each half of the mould was reinforced with 2 aluminium spars which act as an alignment when the parts are glued together. ABS vapour smoothing could not be applied due to larger areas of distortion created during printing. The gaps were then filled with high performance glue containing cotton flocks, as shown in Figure 16.

The process of filling the gaps was repeated several times, with sanding after each step. Subsequently, the entire mould was covered with a single layer of resin to fill the layer line and smooth





(a) Mould gaps due to ABS warping

(b) filled mould gaps

Figure 16 – mould issues during assembly

the surface. After further sanding, 4 layers of carnauba wax were applied. A final layer of PVA was applied for the later removal of the parts. Figure 17 shows each mold half right before lamination.



Figure 17 – Final mould halfs before lamination

4.2.3 Lamination

After laminating 2 layers of GFRP into the mould halves and curing them in a vacuum bag, the only difference compared to the other methods was the gluing of the ribs. Initially, the ribs were prepositioned in the moulds with the spar, then a small drop of glue was applied to secure their position. High performance glue with cotton flocks was then applied using a brush to the spar-rib joints and from rib to skin.

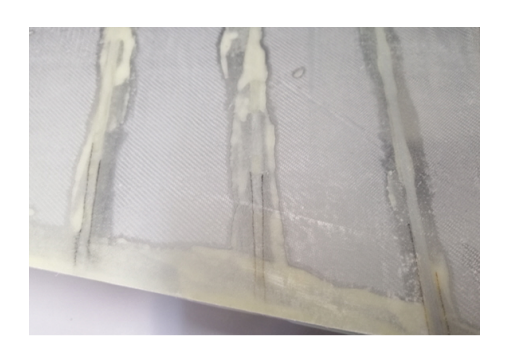
The mould halves were then placed together and closed. Heavy counterweights were placed on the moulds to ensure proper bonding of the glued parts.

4.2.4 Weight Rating M2

Table 7 presents the individual components of M2. Due to the method used, it was not possible to measure the mass of the skin separately before the addition of the cotton flock adhesive. However, assuming that the skin is similar to M1 at 191g, this would give a proportion of 27.8% for the skin of the total mass. The amount of glue is quite high at 85.2g, but it is necessary to bond all the ribs and close the leading and trailing edges. The transparent GFRP skin on the finished wing indicates that most of the adhesive has been applied outside the actual bond area (compare Figure 18). More careful planning of the glue and its application is therefore required.







(b) Bottom side trailing edge

Figure 18 – Foam cutter for styrofoam

Part Name	Mass [g]	Ratio to Total [%]
main spar Ø25	107.9	15.7
2nd spar Ø20	43.1	6.3
2x spar flap Ø6	8.7	1.3
internal ribs		
wing R1-R14	162.1	23.6
8x flaps	20.0	2.9
8x aileron	8.3	1.2
GFRP skin incl. resin & glue		
wing	276.9	40.3
flap	39.8	5.8
aileron	20.2	2.9
total mass	686.9	100

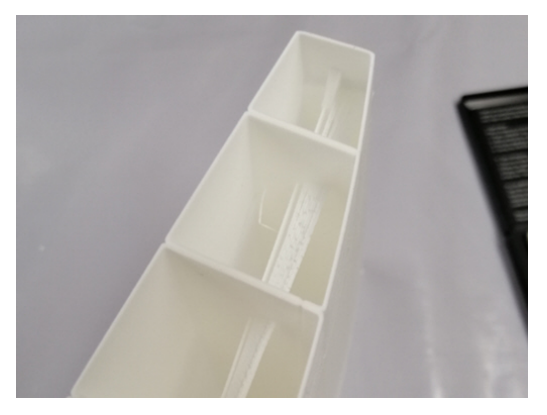
Table 7 – Individual part masses of M2 wing

4.3 M3: 3D Printed Core 4.3.1 Pretest LW-PLA

In order to pre-test the properties of LW-PLA, some test prints were made to evaluate its properties and find any potential problems. Due to the foaming process, the design of the part should be that the nozzle of the printer can run in a continuous loop without retracting or moving to other locations within one print layer. If a movement within a layer is required, there is always be oozing out of the nozzle and this creates the irretation in the print that can be seen in Figure 19a. In addition, this results in too little material when restarting at the next starting point, resulting in a too thin wall thickness and therefore weak parts, as shown in Figure 19b. To prevent this, the design must be adjusted accordingly. Moreover, the movements can be analysed within the slicing software to identify any travelling movement. A further conclusion from this is that only a single part can be printed at a time. To achieve a sufficiently strong skin, the usual nozzle size of 0.4mm is increased to 0.6mm. This ensures the skin is thick enough to provide good impact resistance and can be handled by hand without risk of damage. This is also consistent with the findings of [2].

As an initial analysis, the Fowler flap was printed using different materials to determine achievable masses. Table 8 shows the corresponding values. LW-PLA shows a mass reduction of 49% compared to regular PLA. In addition, the allowance for the inner ribs, related to the circumference, was determined to be 1.92⁵. The weight of the bottom layers was calculated out for this analysis.

⁵in the preceding prediction this allowance was 1.67, which shows the high uncertainty also created by the necessary design reinforcements





(a) Additional material outgrowths

(b) Too thin walls

Figure 19 – Oozing effects while traveling movements

Material	Mass [g]	Ratio to PLA [%]
PLA	50	100
Polylite LW-PLA	37	74
Colorfab LW-PLA	24.3	49

Table 8 – Weight comparisons for a half fowler flap

4.3.2 Printed Core

The wing, flap and aileron were divided into several sections with a maximum height of 200mm. This limit is necessary due to both the size of the printer and the risk of instability during printing, which can lead to wobbling. This wobbling causes less accuracy and weakens the strength of the part. Additional section splits were made at functional edges such as the transition from the flap area to a solid wing area. By printing each part with 4 bottom layers with a total thickness of 1mm, a solid intersection is created where no fibre reinforment is required. These bottom layers also act as solid ribs and torque transmitters. Figure 20 shows the wing sections, printed mainly in black and white LW-PLA for visibility only.



Figure 20 - Printed Section of M3 wing, flap and aileron

In terms of printing time and cost, a total of 35 hours of printing and approximately 470g of LW-PLA were required, resulting in a material cost of 20.05€⁶. 15 individual prints were required with print times varying from 1h to 6h depending on the part. Additionally, it is necessary to consider additional time for cooling of the part in the printing chamber and part change between prints.

⁶cost basis is a colorfabb LW-PLA spool of 750gr for 32€

One of the interests is how big is the deviation in the surcharge for the internal structures. Therefore, 3 sections, as shown in Figure 21, were analysed in detail. An obvious factor is the increase due to the auxiliary spar and the two cable ducts. Furthermore, the reinforcement of the nose section also differs from the previous prediction. The surcharges for each section can be taken from Table 9. To improve future predictions, the following factors can also be taken into account: spar and channel cut-outs, reinforcements in critical areas, floor thickness of each section, and the number of sections.

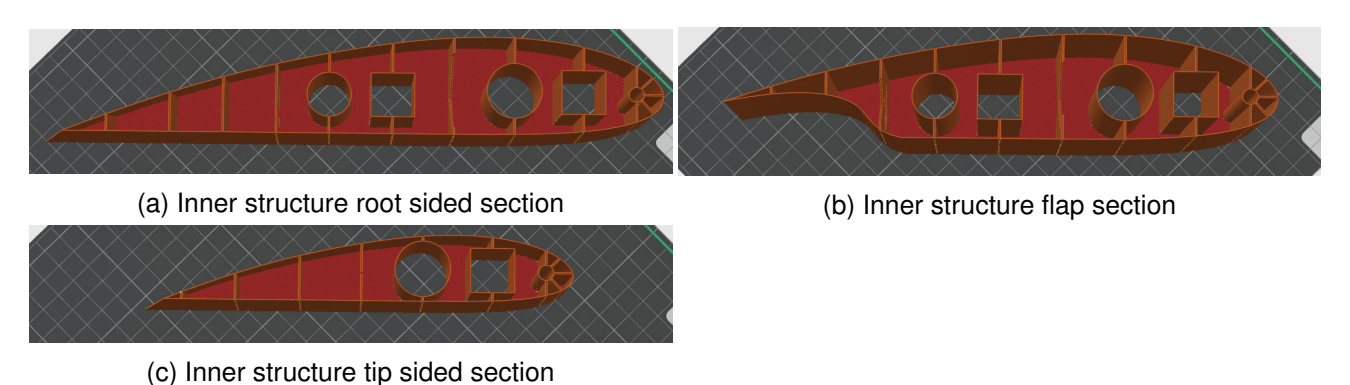


Figure 21 – Inner structures on different wing sections

Section	Surcharge [-]
root sided flap tip sided	2.13 2.39 2.04

Table 9 – Mass surcharges due to inner structures

4.3.3 Lamination

The M3 wing is also laminated as a positive moulding. Prior to lamination, each section and the wing spar were glued in place with a high performance adhesive, along with cotton flocks for the spars and CA adhesive for the printed parts. Contrary to the M1 lamination, the use of Mylar foil was avoided due to the problems with the raised leading edge. A device was built to hold the wing with the leading edge up during lamination (see Figure 22a). The device ensured that the leading edge always had a tight fit. Following lamination, 2 layers of peel ply were applied on top of the GFRP to absorb excess resin. The wing together with the fixture was placed in the vacuum bag during curing, as shown in the Figure 22b.⁷.

Due to the printed internal structures, only a vacuum of -10 kPa could be used. At higher vacuum levels, the original shape between the internal structures began to deform and flatten. Even with this low vacuum at the depth of the cable ducts, the shape of the skin flattened minimally. Looking at the inner structures in Figure 21, it can be seen that the design over the cable ducts was not load optimised, as there is no straight line from the top to the bottom of the wing.

After curing and removal of the peel ply, the wing skin was left with this rough finish. A further top coat would certainly improve the aerodynamic efficiency, but was not prioritised for structural testing as the focus was primarily on structural integrity rather than cosmetic appearance.

4.3.4 Weight Rating M3

The Table 10 presents the actual weights of the components. Interestingly, the skin mass is similar to the other methods. Less adhesive was required due to the fitting geometry of each printed part.

⁷The edges of the fixture as well as the screws should be protected by at least two layers of breather cloth to ensure that the vacuum bag is not damaged



(a) Lamination fixture for M3 wing

(b) Laminated M3 wing in vacuum bag

Figure 22 – Lamination orientation for M3 wing

However, the printed parts themselves are quite heavy. This is mainly due to the internal structures and the use of a 0.6mm nozzle.

Part Name	Mass [g]	Ratio to Total [%]
main spar Ø25	108.4	12.8
2nd spar Ø20	42.6	5.0
2x spar flap Ø6	9.8	1.2
printed parts		
wing R1-R11	365.5	43.1
flap	49.3	5.8
aileron	24.4	2.2
glue with cotton flakes GFRP skin incl. resin	15.5	1.8
wing	193.0	22.8
flap	33.1	3.9
aileron	12.8	1.5
total mass	848.3	100

Table 10 – Individual part masses of M3 wing

4.4 Interim Conclusion

With each method, the wing geometry could be produced. All 3 wings are shown in Figure 23. The cutout for the aileron in M1 is still to be made, but is postponed for future load tests to see the effect on the actual stability of the wing. Table 11 displays the total masses of each wing. Starting with M1 as the lowest, followed by M2 with a mass increase of 12.8 % and M3 with an increase of 39.3 %. This is slightly different from the previous prediction.

Please note that the Table 11 does not include the cost of tools such as the vacuum pump, foam cutter, cutting and grinding tools, mixing cups and brushes.

In addition, different linkages for the aileron refer to suitable hinges from the method. The flap mechanism is omitted from the load tests as it is not of interest at this stage.

Feature	Unit	M1	M2	М3
Total mass per wing Normalized mass Ratio to group lowest	g g/m %	609 761 100	687 858 112.8	848 1060 139.3
Total costs per wing Cost for core (incl. stencil/moulds) (excl. spars)	€ €	95 32	210.8 121.5	106.4 19
Total lead time	d	1.5	6.5	3.5

Table 11 – Actual key figures of each method for the built wing

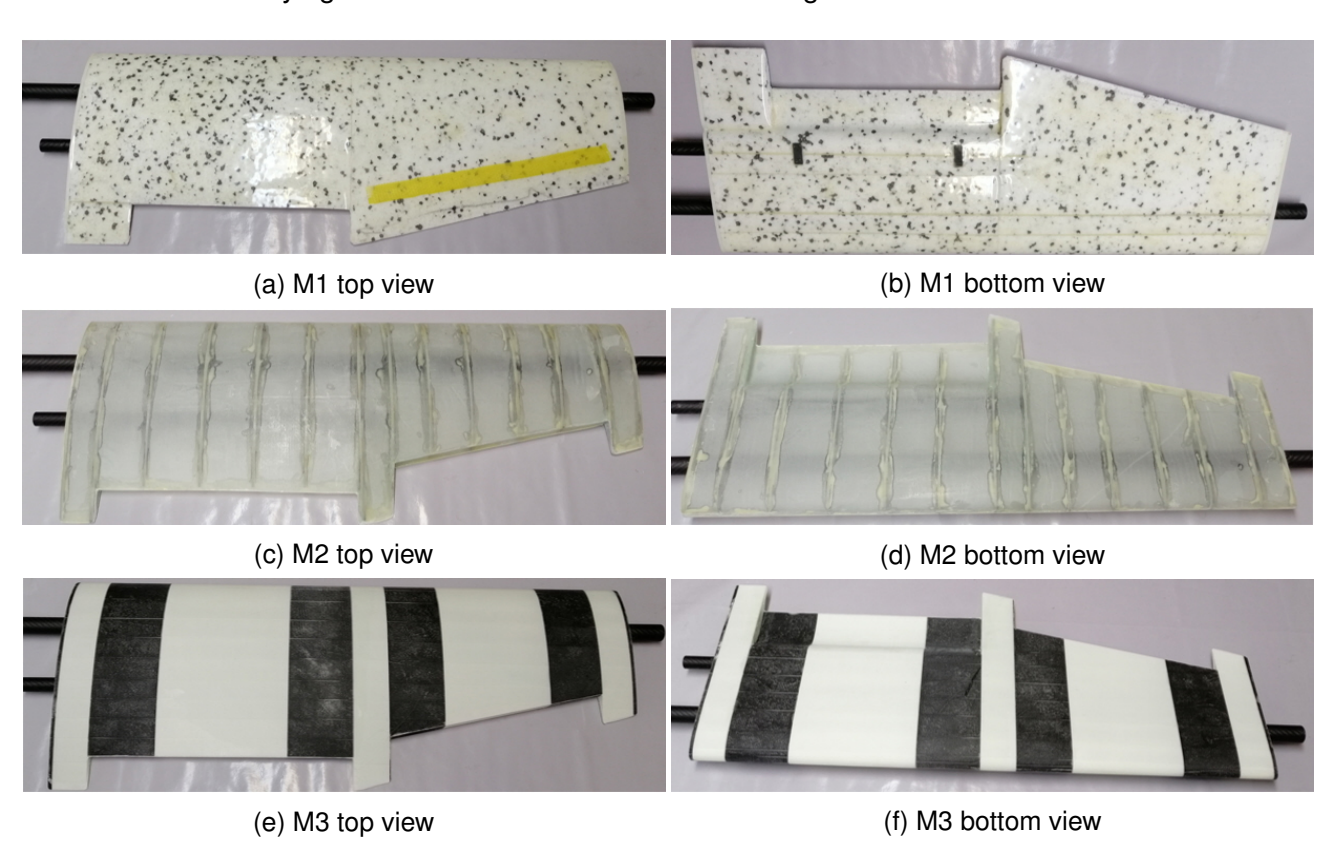


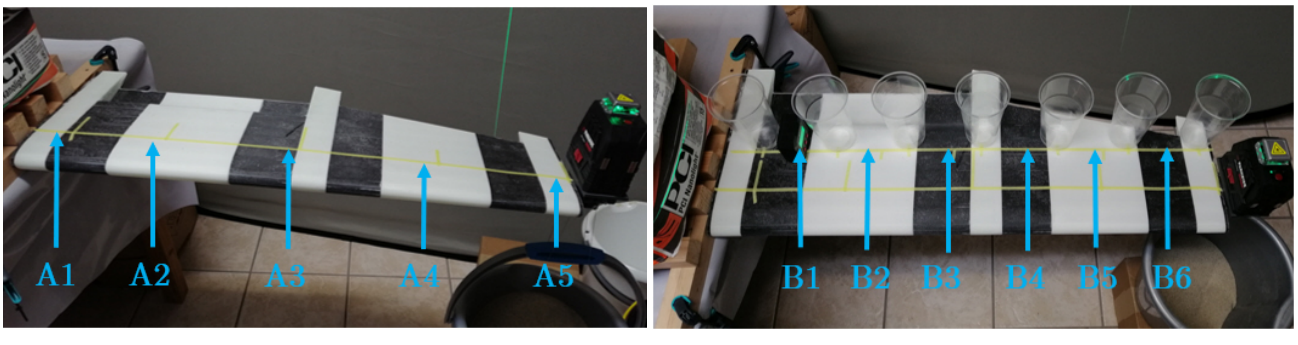
Figure 23 – Finished wings of each method

5. Stress Tests

5.1 Test Setup

A wooden fixture with holes for the main and auxiliary spar was prepared for the load test. The fixture was loaded with an additional 60kg to compensate for the loads on the wing. Angular deviations from the fixture under load were later calculated to obtain only the wing deflection.

An ABS print was placed on the wing tip side of each method to apply forces. A cross line laser was also placed on top to measure the absolute deflection of the wingtip. Angular deflection was measured at several positions on the wing as shown in Figure 24. For the hover tests, the spanwise angle deflection was measured and located from A1-A5 (refer to Figure 24a). For the cruise tests, the angular deflection orthogonal to the span was measured at positions B1-B6 (refer to Figure 24b). The angle measuring device had to be moved to the measuring points each time which introduced an uncertainty of approximately 0.05-0.1° into the results.



(a) Hover Setup

(b) Cruise Flight Setup

Figure 24 – Setups for different load cases

5.2 Loadcases

5.2.1 Hover

For the hover load case, a static load was applied to the wingtip, starting with 6kg and followed by 2kg steps up to 14kg. Figure 25 shows the angular deflection of M1 for the predefined measurement positions. As can be seen, the deflection increases almost linearly. This trend was also observed for the other methods. For A2 to A5 the angular deflection of A1 (root) has been subtracted to remove movement in the fixture.

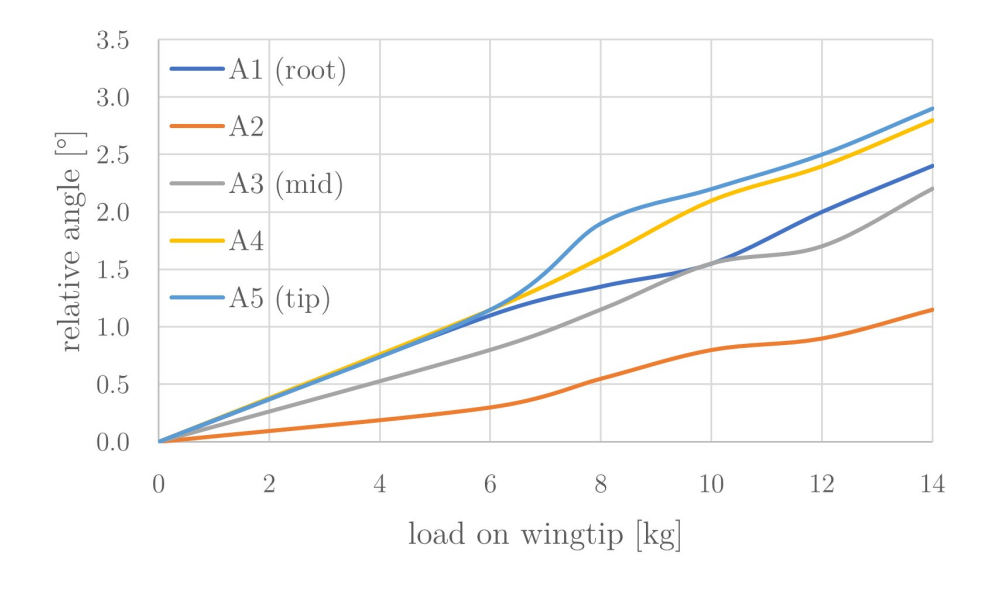


Figure 25 – Wingbending of M1 in hovertest

Feature	Unit	M1	M2	М3
max deflection on tip	mm	30.4	25.4	28.1
normalized deflection	mm/kg	2.91	2.86	2.23
ratio deflection to M1	%	100	98.5	76.6
normalized angle delta on tip ratio angle delta to M1	%kg	0.21	0.295	0.195
	%	100	140	92.9

Table 12 - Key figures from loadcase hover

The results of the hover load test are summarised in Table 12. The maximum angle of deflection was

4.1° for M2. However, M2, in particular, experienced a lot of buckling of the upper skin of the wing, as presented in Figure 26. This certainly influenced the angle measurements of M2.

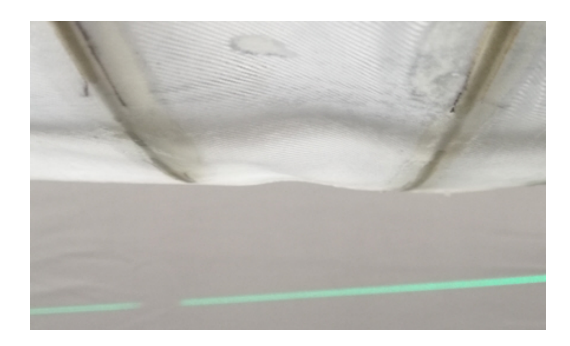


Figure 26 – Buckling of the upper skin of M2 during load

5.2.2 Cruise

To simulate cruise flight, cups filled with sand were placed according to the lift distribution over the wing as shown in Figure 27a. The approach is similar used in [28]. An angle gauge was placed between each cup to measure the angular deflection. As can be seen in the Figure, the cups had to be stacked to simulate the lift in cruise flight. In a second test, to measure a higher torque than in cruise flight, the buckets were moved further towards the trailing edge (100mm from main spar). The results of this test are shown in the high torque test.



(a) Load distribution according to lift distribution

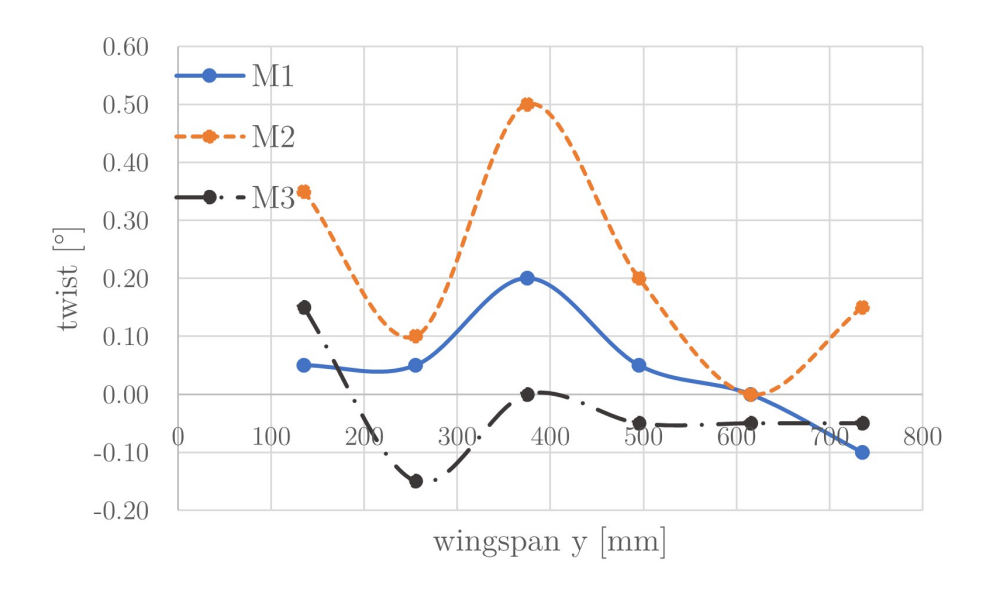
(b) ultimate load test with 30kg

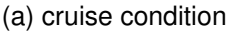
Figure 27 – Wing twist over the wingspan for different loadcases

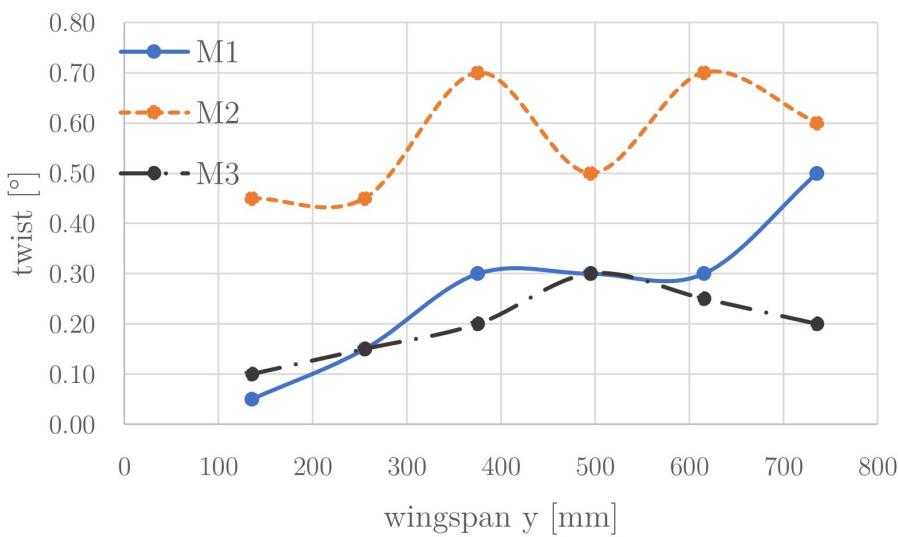
The results in Table 13 show that the mean twist of M1 and M3 in cruise flight have a very low value, which is already within the measurement uncertainty. In the high torque test, M3 gives the lowest twist, followed by M1. Surprisingly, M2 shows the highest twist, even with the CFRP reinforced ribs. The detailed angle deflections of each measuring position are shown in Figure 28.

Feature	Unit	М1	M2	М3
simulated loads: lift cruise torque high torque	kg kgmm kgmm	9.5 285 950	9.5 285 950	9.5 285 950
mean twist for: cruise high torque	0	0.04 0.27	0.22 0.57	-0.02 0.20

Table 13 – Key figures from twist testing







(b) high torque condition

Figure 28 – Wing twist over the wingspan for different loadcases

In a final test, the ultimate load factor was tested with n_{lim} =3. Sandbags were used as shown in Figure 27b. A disadvantage here is that the torsion (B1-B6) could not be measured. A1 and A5* were measured as well as the tip deflection ⁸. Figure 29 shows the tip deflection under ultimate load. The angular displacement from the fixture has been calculated and subtracted. Please treat the result with caution as the absolute deflection of M1, M2 and M3 were similar with a spread of 4mm.

6. Conclusion

The objective of this paper was to provide a guide for other researchers/developers starting to incorporate 3D printing into their composite design. Therefore, the weight prediction could be refined with the practical approach of building smaller test wings. After all, method M1 provides the lowest weight for the desired wing. But more complicated shapes and curves are difficult to model. The method is really good for simpler wing shapes without flaps or transitions. As a result, M1 is suitable for most empennage parts or almost straight wings. Method M2 still reaches a good weight performance, but the moulding costs and lead times are the worst compared to the others. Furthermore the skin thick-

⁸A5* means that the angle gauge was positioned on the laser platform for measurement

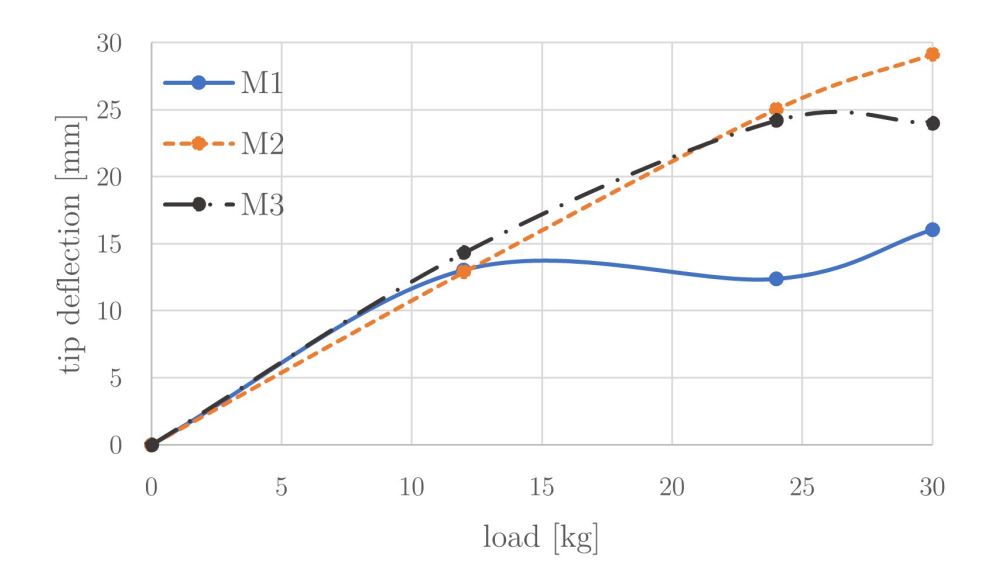


Figure 29 - Tip deflection during ultimate load test

ness must probably be thicker due to buckling effects. But it can be used to produce very complex shapes where local reinforcement is required. M2 is best suited for complex wing structures with control surfaces and hollow fuselage structures where space is mandatory. Method M3, the heaviest of the group but with the best twist stiffness, provides the most flexibility, which could be used for fast iterations in practical approaches. It is therefore most suitable for payload compartments, but also for landing gear structures.

6.1 Outlook

Further research will focus on applying the appropriate method to compatible parts of the aircraft under consideration, which is still in the design process. The collected data will also be used for this purpose.

Furthermore, the built wings will be tested in a dynamic behaviour. To this end, each wing will be mounted on a test rig that is attached to a car trailer. The use of the trailer should help in case a windtunnel infrastructure is not available due to time constraints.

New tests will be carried out on the M2 ribs, mainly to simplify the process of adding the CFRP rowing to the rib, but also to achieve the same rib qualities. In addition, the M2 skin is varied with a printed honeycomb pattern to create a sandwich structure to improve buckling resistance.

Then the aileron and flap mechanism will also be considered for load testing.

Contact data author via mailto: thomas.mueller.ilt@tuhh.de or phone: +49 40 42878 4447

7. Copyright Statement

The authors confirm that they, and/or their company or organization, hold copyright on all of the original material included in this paper. The authors also confirm that they have obtained permission, from the copyright holder of any third party material included in this paper, to publish it as part of their paper. The authors confirm that they give permission, or have obtained permission from the copyright holder of this paper, for the publication and distribution of this paper as part of the ICAS proceedings or as individual off-prints from the proceedings.

References

- [1] Baker A., Dutton S., Kelly D. *Composite Materials for Aircraft Structures*. 2nd edition, American Institute of Aeronautics and Astronautics, 2004.
- [2] Skawiński, I. and Goetzendorf-Grabowski, T. (2019), "FDM 3D printing method utility assessment in small RC aircraft design", Aircraft Engineering and Aerospace Technology, Vol. 91 No. 6, pp. 865-872. https://doi.org/10.1108/AEAT-07-2018-0189

- [3] Martinez, Dan William, et al. "A Comprehensive Review on the Application of 3D Printing in the Aerospace Industry." Key Engineering Materials, vol. 913, Trans Tech Publications, Ltd., 18 Mar. 2022, pp. 27–34. Crossref, doi:10.4028/p-94a9zb.
- [4] Ferretti P., Santi G.M., "Production readiness assessment of low cost, multi-material, polymeric 3D printed moulds", Heliyon, Volume 8, Issue 10, 2022, ISSN 2405-8440, https://doi.org/10.1016/j.heliyon.2022.e11136.
- [5] Ferretti, P.; Santi, G.M.; Leon-Cardenas, C.; Freddi, M.; Donnici, G.; Frizziero, L.; Liverani, A. Molds with Advanced Materials for Carbon Fiber Manufacturing with 3D Printing Technology. Polymers 2021, 13, 3700. https://doi.org/10.3390/polym13213700
- [6] Bere, P.; Neamtu, C.; Udroiu, R. Novel Method for the Manufacture of Complex CFRP Parts Using FDM-based Molds. Polymers 2020, 12, 2220. https://doi.org/10.3390/polym12102220
- [7] Munoz-Guijosa, J.M.; Zapata Martínez, R.; Martínez Cendrero, A.; Díaz Lantada, A. Rapid Prototyping of Personalized Articular Orthoses by Lamination of Composite Fibers upon 3D-Printed Molds. Materials 2020, 13, 939. https://doi.org/10.3390/ma13040939
- [8] Pawlak W., Low cost production of laminating mold with use of 3D printing technology, 2018, https://www.researchgate.net/publication/330003077
- [9] Acanfora V., Sellitto A., Experimental investigation on 3D printed lightweight sandwich structures for energy absorption aerospace applications, Aerospace Science and Technology, Volume 137, 2023, 108276, ISSN 1270-9638, https://doi.org/10.1016/j.ast.2023.108276.
- [10] Kumar A.P., Sadasivuni K.K. *HIGH-PERFORMANCE COMPOSITE STRUCTURES*. 1st edition, Springer, 2022
- [11] NACA 4 digit airfoil generator (NACA 4416 AIRFOIL), airfoiltools.com, accessed on 15.04.2024, http://airfoiltools.com/airfoil/
- [12] LOW-SPEED AERODYNAMIC CHARACTERISTICS OF NACA 6716 AND NACA 4416 AIR-FOILS WITH 35-PERCENT-CHORD SINGLE-SLOTTED FLAPS, nasa.gov, accessed on 01.04.2024, https://ntrs.nasa.gov/api/citations/19740013521/downloads/19740013521.pdf
- [13] Gundlach J. *Designing Unmanned Aircraft Systems*. 2nd edition, American Institute of Aeronautics and Astronautics, 2014.
- [14] Lutz T.; Universität Stuttgart: Skript zu den Vorlesungen Flugzeugaerodynamik I & II; 2017
- [15] Strohmeyer A. Flugzeugentwurf II. Rev 1.03, University of Stuttgart, 2020
- [16] Lastannahmen nach CS-VLA, www.amateurflugzeugbau.at, accessed on 01.05.2024, https://www.amateurflugzeugbau.at/fileadmin/inhalte/flugzeugbau/technik/Vortrag_Lastannahmen.pdf
- [17] Pfefferkorn D. Entwicklung und Bau eines Vollkunststoff-F3B-Modells. 1st edition, Neckar-Verlag, 1993.
- [18] HOW TO PRINT WITH LW-PLA, colorfabb.com, accessed on 04.12.2023, https://colorfabb.com/how-to-print-with-lw-pla
- [19] ColorFabb LW-PLA Testing Foaming PLA, cnckitchen.com, accessed on 04.12.2023, https://www.cnckitchen.com/blog/colorfabb-lw-pla-testing-foaming-pla
- [20] Upgrading from LW-PLA to LW-PLA-HT, colorfabb.com, accessed on 04.12.2023, https://colorfabb.com/de/upgrading-from-lw-pla-to-lw-pla-ht-what-you-need-to-know
- [21] Polylite LW-PLA, polymaker.com, accessed on 15.05.2024, https://polymaker.com/product/polylite-lw-pla/
- [22] PolySmooth, check for datasheet, polymaker.com, accessed on 06.12.2023, https://polymaker.com/product/polysmooth/
- [23] Polylite LW-PLA, polymaker.de, accessed on 18.05.2024, https://polymaker.com/wp-content/tech-docs/PolyLite_LW_PLA_PIS_EN.pdf
- [24] Verstärkungsfasern Einführung und Überblick, r-g.de, accessed on 18.05.2024, https://www.r-g.de/wiki/Verst%C3%A4rkungsfasern_-_Einf%C3%BChrung_und_%C3%9Cberblick
- [25] Acrylnitril-Butadien-Styrol-Copolymer (ABS), kunststoffe.de, accessed on 18.05.2024, https://www.kunststoffe.de/a/grundlagenartikel/acrylnitril-butadien-styrol-copolymer-ab-311439
- [26] Lambie J. COMPOSITE CONSTRUCTION FOR HOMEBUILT AIRCRAFT. 1st edition, Aviation Publishers, 1985.
- [27] Mouldless Motorsport Wing Construction, easycomposites.eu, accessed on 15.04.2024, https://www.easycomposites.eu/learning/mouldless-carbon-fibre-aero-wing
- [28] D3.9 Advanced wing integration and ground test completed, flipased.eu, acressed on 28.05.2024, https://flipased.eu/deliverables/FLIPASED_D3_9.pdf